Current Research in Food Science 7 (2023) 100550

Contents lists available at ScienceDirect

Current Research in Food Science

journal homepage: www.sciencedirect.com/journal/current-research-in-food-science

Adsorption and controlled release performances of flavor compounds by rice bran insoluble dietary fiber improved through steam explosion method

Hongcheng Liu [a,b,1], Dilinuer Ainiwan [a,c,1], Yingxu Liu [a,b], Xiaolan Dong [a,c], Hongxiu Fan [a,b], Tong Sun [a,d], Pingyun Huang [a,d], Shanshan Zhang [a,d], Dawei Wang [a,c], Tingting Liu [a,c,*], Yanrong Zhang [a,b,**]

[a] School of Food Science and Engineering, Jilin Agricultural University, Changchun, 130118, PR China
[b] Scientific Research Base of Edible Mushroom Processing Technology Integration of Ministry of Agriculture and Rural Affairs, Changchun, 130118, China
[c] Engineering Research Center of Grain Deep-processing and High-Efficiency Utilization of Jilin Province, Changchun, 130118, China
[d] Key Laboratory of Technological Innovations for Grain Deep-processing and High-Efficiency Utilization of By-Products of Jilin Province, Changchun, 130118, China

ARTICLE INFO

Handling Editor: Dr. Xing Chen

Keywords:
rice bran insoluble dietary fiber
Steam explosion treatment
Flavor adsorption
Flavor release profile
HS-SPME GC/MS
Electronic nose

ABSTRACT

In this study, steam explosion was employed as a modification process for rice bran insoluble dietary fiber (RBIDF) to improve the flavor adsorption and controlled release capacities of RBIDF. Results showed that the flavor adsorption ability of RBIDF was effectively improved due to the unfolding structure, increased specific surface area and pore volume and exposure of more functional groups after steam explosion treatment. The mechanism of the flavor adsorption behavior of modified RBIDF was preliminarily explored using adsorption kinetics and isotherms combined with SEM and DSC analysis. Results showed that the Langmuir isotherm model and pseudo-second-order kinetic model yielded the best fit to the adsorption data, indicating monolayer adsorption of flavor onto the modified RBIDF, and the adsorption was mainly driven by chemisorption process. The flavor release profile of modified RBIDF was investigated by HS-SPME/GC-MS and E-nose. After long-time storage, the flavor compounds were retained at a higher concentration in the modified RBIDF compared with the untreated RBIDF, indicating that the steam explosion treatment prolonged the retention time and enhanced the retention and controlled release capacities of RBIDF for flavor compounds. This study provides indications for potential applications of steam explosion-modified RBIDF as a novel flavor delivery system and functional ingredient.

1. Introduction

Flavor is a very important characteristic of foods and it influences the consumer sensory perception and product acceptability. Flavor substances such as essential oils and flavoring agents are small molecular volatile compounds, which are widely used to improve the sensory quality of the products (Liu et al., 2022; Premjit et al., 2022). However, most flavor substances are usually highly volatile and are prone to degradation under conditions of food processing or thermal treatments such as heating and sterilization. Therefore, it is vital to retain the flavor compounds stably during food manufacturing and storage processes. In addition, the controlled release property of flavor is also desired during storage. Adsorption technique is one of the most widely employed methods for increasing shelf-life of flavor compounds and protecting them from environmental agents (Han et al., 2021). The advantages of adsorption method include ease of use, high efficiency and low cost. Adsorbents are usually porous organic or inorganic materials, with large specific surface area, easily regenerated, adjustable surface property and relatively simple process. They play a critical role in the adsorption of flavor compounds. Nowadays, development of non-toxic, degradable and low-cost adsorbents with flavor binding capacity using by-products of food processing show great potential in the field of adsorption.

Rice bran is an underutilized byproduct of rice milling. Approximately 74 million tons of rice bran are produced annually, most of which are either discarded or used for animal feed. Rice bran contains 35%–50% dietary fiber, and nearly 90% of the total dietary fiber is insoluble

* Corresponding author.School of Food Science and Engineering, Jilin Agricultural University, Changchun, 130118 China.
** Corresponding author.School of Food Science and Engineering, Jilin Agricultural University, Changchun, 130118 China.
E-mail addresses: liutingting@jlau.edu.cn (T. Liu), zhangyanrong0044@jlau.edu.cn (Y. Zhang).
[1] These authors contributed equally to this work.

https://doi.org/10.1016/j.crfs.2023.100550
Received 5 May 2023; Received in revised form 3 July 2023; Accepted 12 July 2023
Available online 20 July 2023

(Zhao et al., 2018), indicating that rice bran insoluble dietary fiber might be an excellent source of insoluble dietary fiber. Hemicellulose, cellulose and lignin are the three main components of RBIDF, and the surface of these components usually contains a large number of functional groups such as hydroxyl, phenol hydroxyl, aldehyde, ketone, ester and carboxyl groups, which can have certain adsorption capacities for some molecules such as lipids, glucose, cholesterol and heavy metal ions (Niu et al., 2023; Wu et al., 2021a). Previous study has proven that RBIDF had a good ability to adsorb Cd ion in vitro. The hydroxyl, carboxyl and NH groups of RBIDF are the main functional groups, which can chemically bind with Cd (Wu et al., 2021b). Niu et al. reported that RBIDF after ball milling processing had higher glucose and cholesterol adsorption capacities and oil holding capacity. This might be due to the fact that the ball milling treatment result in higher porous matrix structure, increased surface hydrophobicity and exposure of more functional groups (such as hydroxyl, carbonyl, etc.) (Niu et al., 2023).

We are interested in the application of RBIDF as a host material for flavor compounds. Since BRIDF has porous structure and contains functional groups, it is reasonable to expect the flavor compound would be enclosed in the three-dimensional network structure and bind to the functional groups in the matrix. However, RBIDF usually has a compact polymeric structure, which is difficult to disintegrate to expose functional groups (Wu et al., 2021b). Therefore, the compact structure must be disrupted in a controlled manner to produce insoluble dietary fiber with the desired structural and functional properties. Steam explosion was one of the most effective methods to disrupt lignocellulosic structure in an environmentally friendly way. Researches have also shown that steam explosion could generate cavities or micropores inside the fiber matrix, loosen the cell wall microstructure, and improve cholesterol and ion adsorption capacities (Ouyang et al., 2023a; Vitrone et al., 2022; Wang et al., 2021). Therefore, in this research, steam explosion technology will be introduced to modify RBIDF and improve functional properties.

The objective of this study is to study the adsorption and desorption behaviors of flavor molecules into RBIDF in order to evaluate the impact of the modification on the ability of RBIDF to retain the flavor compounds. Red date flavoring agent, which is widely used in foods such as baking product, dairy product and snacks, was used as the absorbate in this study. Brunauer–Emmett–Teller (BET) surface area analysis, scanning electron microscopy (SEM), and Fourier transform infrared (FTIR) spectroscopy, differential scanning calorimetry (DSC), adsorption kinetics and isotherms were used to study the adsorption characteristics and mechanism of flavor molecules into RBIDF before and after the modification. Additionally, the characteristics of controlled release of flavor molecules from RBIDF was studied based on headspace solid-phase microextraction coupled to gas chromatography-mass spectrometry (HS-SPME/GC-MS) and electronic nose (E-nose). This study could provide new insights for the modified preparation of dietary fiber as a novel functional ingredient.

2. Materials and methods

2.1. Materials and chemicals

Fresh rice bran was provided by Jilin Nongfu Rice Industrial Co., Ltd. (Jilin, China). Alcalase 2.4 L (2.4 AU/g) was purchased from Novo Enzyme Co. (Bagsvaerd, Denmark). α-Amylase (20000Units/g) was purchased from Pangbo Biological Engineering Co., Ltd. (Nanning, China). Red date flavoring agent was purchased from Shanghai Yuwen Flavor & Fragrance Technology Co., Ltd. (Shanghai, China). The internal standard (2-methyl-3-heptanone) was purchase from McLean Biochemical Technology Co., Ltd. (Shanghai, China). The authentic standards for analysis, *n*-alkane standards (C_7–C_{25}) were purchased from J&K Scientific (Beijing, China). Other chemicals were analytical grade and bought from Beijing Chemical Reagents Co. (Beijing, China).

2.2. Preparation and steam explosion treatment of rice bran insoluble dietary fiber

Rice bran was defatted using supercritical CO_2 extraction method (Nantong Huaan Supercritical Extraction Co., Ltd., Jiangsu, China) at 20 MPa, 40 °C for 2 h (Moreira et al., 2023). Insoluble dietary fiber was extracted from the defatted rice bran by using enzymatic method according to the described procedure (Li et al., 2020). Briefly, the defatted rice bran was incubated with 1% α-amylase at 95 °C for 30 min for removing starch. The mixture was centrifuged at 3800 rpm for 15 min to remove hydrolysis products of starch. The residue was incubated with 1% Alcalase at 60 °C for 4 h for removing protein. After centrifugation, the residue was washed by deionized water for three times. Finally, the obtained RBIDF was dried at 50 °C for 2 days and storied at 25 °C for further use.

Steam explosion treatment of RBIDF was performed using a steam explosion apparatus (QBS-80, Hebi Zhengdao bioenergy Co., Ltd., China) according to our previous studies. Briefly, insoluble dietary fiber of rice bran (400 g) was adjusted to a moisture content of 3% and treated with steam explosion under a pressure of 2.5 MPa for 300 s. The reaction system was terminated with a suddenly explosion by opening outlet ball valve and spraying the sample into the reception chamber. Then the steam exploded rice bran insoluble dietary fiber (SRBIDF) powders were obtained, and the native RBIDF powders obtained with the same procedure without steam explosion treatment was performed as control.

2.3. Structural characterization of RBIDF

The adsorption related characteristics such as specific surface area, pore volume and size were determined with N_2-adsorption/desorption isotherms using an automated specific surface area analyzer (ASAP2020M, Micromeritics Instruments, USA) at a temperature of −196 °C. The N_2 adsorption data were interpreted using the BET model to calculate the specific surface area (SSA) (Brunauer et al., 1938). The pore diameter (PD) and pore volume (PV) were automatically calculated based on different adsorption models, such as Barrett Joyner Halenda model and Density Functional Theory model (Barrett et al., 1951).

A scanning electron microscope (Pro, Phenom-Scientific, Netherlands) was employed to analyze the microstructure of untreated and modified rice bran insoluble dietary fiber. The micrographs of the samples were obtained at an acceleration voltage of 5 kV. The FTIR spectra was recorded in the wavenumber range of 4000 to 400 cm^{-1} with a resolution of 4 cm^{-1} using a Nicolet iS20 FTIR spectrophotometer (Thermo Electron Corporation, USA) to investigate the effect of steam explosion on functional groups of rice bran insoluble dietary fiber. Thermal transitions characteristics of rice bran insoluble dietary fiber samples were analyzed using a differential scanning calorimeter (DSC25, TA Instruments, USA). Each sample (about 6 mg) was weighed into a DSC aluminum pan, sealed and heated from 50 °C to 300 °C at a rate of 10 °C/min with nitrogen as the protective gas (Li et al., 2017). The enthalpy (ΔH) and peak temperatures (T_p) were calculated from the DSC curves using the Trios software version 2.0.

2.4. Flavor adsorption capacity of RBIDF under different pH values, temperatures and with different particle sizes

Adsorbate solution containing 0.35 mg/mL red date flavoring agent was prepared by dissolving 175 g red dated flavoring agent into 500 mL of ethanolic solution (the water-to-ethanol volume ratio was 70:30). Then 0.3 g of the absorbent (RBIDF) was taken in 10 mL of adsorbate solution and the suspension was shaken at 120 rpm for 4 h in a constant temperature shaker. The adsorbate solution was separated from adsorbent particles by passing through a 0.45 μm filter. The residual amount of red date flavoring agent in the filtrate after adsorption was quantitatively determined using a TV-1901 spectrophotometer (Beijing Puxi General Instrument Co., Ltd., Beijing, China) at the wavelength of 215

nm. The amount of red date flavoring agent adsorbed on RBIDF or the adsorption capacity was calculated using Eq. (1):

$$Q = \frac{(c_1 - c_2)v}{m} \quad (1)$$

where Q is the amount of red date flavoring agent adsorbed onto RBIDF in milligram per gram (mg/g), c_1 and c_2 are the initial and equilibrium concentrations of red date flavoring agent (mg/L), v is the volume of red date flavoring agent solution (L), and m is the amount of adsorbent (g) (Ali et al., 2022).

Batch experiments were performed to investigate the adsorption capacity of red date flavoring agent by RBIDF at various temperatures, pH values and with different particle sized absorbents. In this experiment, the particle size of absorbents was 40, 60, 80, 100, 120 and 140 mesh, the pH of the suspension was 2, 3, 4, 5, 6, 7, 8 and 9, and the temperature of the adsorption process was 25 °C, 35 °C, 45 °C, 55 °C and 65 °C.

2.5. Kinetics of flavor adsorption on RBIDF

To investigate the adsorption kinetics of red date flavoring agent on RBIDF, the RBIDF samples (absorbent) were passed through a 100 mesh sieve. Then 0.3 g of RBIDF was taken in 10 mL of 0.35 mg/mL red date flavoring agent solution and the pH of the suspension was adjusted to 5. The samples were shaken in a shaker at 120 rpm and 35 °C for 0.5, 1.0, 1.5, 2.0, 2.5, 3.0, 4.0, 6.0 and 8.0 h. After incubation for different time, the absorbent particles were separated from adsorbate solution with filtration. Then the filtrate was collected for the measurement of the residual amount of red date flavoring agent for the specific time interval. The kinetic data of red date flavoring agent adsorption onto RBIDF was analyzed by fitting with the pseudo-first-order kinetic and pseudo-second-order models. The pseudo-first-order kinetic model is given by Eq. (2):

$$In(Q_e - Q_t) = InQ_e - k_1 \quad (2)$$

where Q_t and Q_e are the amounts of red date flavoring agent adsorbed at time t, and at equilibrium respectively for per mass of RBIDF (mg/g), t is the adsorption time (h), k_1 is the rate constant of pseudo first-order adsorption (h^{-1}). The values of Q_e and k_1 can be calculated from the linear plot of In(Q_e-Q_t) *vs* t.

The pseudo-second-order model is given by Eq. (3):

$$\frac{t}{Q_t} = \frac{t}{Q_e} + \frac{1}{k_2 Q_e^2} \quad (3)$$

where k_2 is the rate constant of pseudo-second-order adsorption (g/(mg·h)). The values Q_e and k_2 can be calculated from the linear plot of t/Q_t *vs* t (Hu et al., 2022).

2.6. Isotherms of flavor adsorption onto RBIDF

To examine the affinity of red date flavoring agent toward the RBIDF adsorbents, the adsorption isotherm experiment was performed. 0.3 g of RBIDF sample with 100 mesh size was added into 10 mL adsorbate solution with different concentrations (50–650 mg/L), and incubated at 35 °C for 4 h. The adsorption equilibrium data of red date flavoring agent onto RBIDF samples were used to fit with the Freundlich and Langmuir isotherm models. The Freundlich isotherm model can be expressed by the following equation:

$$InQ_e = InK_f + \frac{1}{n} InC_e \quad (4)$$

where Q_e is the amount of red date flavoring agent adsorbed at equilibrium for per mass of RBIDF (mg/g), C_e is the equilibrium concentration of red date flavoring agent in the solution (mg/L), K_f is the Freundlich nonlinear coefficient related to the adsorption capacity ((mg/g)/(L/mg)$^{1/n}$), n is the Freundlich constant related to the adsorption intensity. The n and K_f values can be determined from the linear plot of InQ_e *vs* InC_e.

The Langmuir isotherm model can be expressed by the following equation:

$$\frac{C_e}{Q_e} = \frac{C_e}{Q_{max}} + \frac{1}{K_L Q_{max}} \quad (5)$$

where Q_{max} is the Langmuir constant indicating the maximum monolayer adsorption capacity of absorbent (mg/g). K_L is the Langmuir constant related to the free energy of adsorption (L/mg). The values of Q_{max} and K_L can be calculated from the linear plot of C_e/Q_e *vs* C_e (Wang et al., 2022).

2.7. Flavor release behavior from RBIDF

When the adsorption of red date flavoring agent had reached equilibrium, desorption experiments were performed to investigate the release behavior of flavor from RBIDF and SRBIDF absorbents. RBIDF and SRBIDF samples obtained from the flavor adsorption experiments (0.6 g) were placed into a 20 mL open headspace vials and incubated in a water bath at 25 °C for 0, 7, 14, 21 and 28 days respectively. After the incubation, the samples were cooled in an ice bath, sealed tightly and used for HS-SPME/GC-MS analysis.

2.7.1. Analysis of flavor by HS-SPME/GC-MS

The headspace flavor compounds desorbed from RBIDF and S-RSIDF were sampled by means of solid-phase microextraction (SPME) (Xiao et al., 2022). The SPME fiber needle (DVB/CAR/PDMS, 50/30 μm) was exposed to the headspace of 0.6 g of each sample for 30min at 50 °C. After absorption, the SPME fiber needle was injected into the gas chromatography (GC) inlet (240 °C) to desorb for 4 min. The volatile compounds were separated using a HP-INNOWax capillary column (30 m × 0.25 mm × 0.25 μm). The temperature gradient of GC oven was set as follows: initial temperature 40 °C maintained for 4 min, increased at 5 °C/min to 150 °C, then increased to 230 °C at 10 °C/min, and the final temperature was held for 10 min. The helium flow rate was set as 1.0 mL/min and the injection mode was split (5:1). The injector temperature, ion source temperature and transfer line temperature were 240 °C, 250 °C and 240 °C, respectively. The mass spectrometer was operated in a mass scan range of 35–500 amu.

Flavor compounds desorbed from the absorbents were qualitatively determined by comparing their retention time and mass spectra with those of the available authentic standards. Flavor compounds without authentic standards were tentatively identified by matching their mass spectra with the data in the NIST MS Search 2.3 database and by comparing their retention indices (RIs) with the literature values. The RI values were determined by running the standard *n*-alkanes (C_7–C_{25}) under the above chromatographic conditions (Zheng et al., 2023). The contents of flavor compounds were determined based on the semi-quantitative method using 2-methyl-3-heptanone (81.6 μg/mL in methanol) as an internal standard, according to previously reported methods (Xia et al., 2017).

Odor activity value (OAV) is the ratio of concentration of each flavor compound to the odor threshold value of the flavor compound from literature. It can be used to assess the contribution of each volatile compounds to the overall flavor of samples. The flavor compound with an OAV>1 is considered significant for the odor characteristic (Zhao et al., 2021).

2.7.2. Analysis of flavor by E-nose

E-nose analysis was conducted according to a previous study with minor modification (Fan et al., 2023). A portable electronic nose (PEN 3 Airsence, Schwerin, Germany) was equipped with ten metal oxide

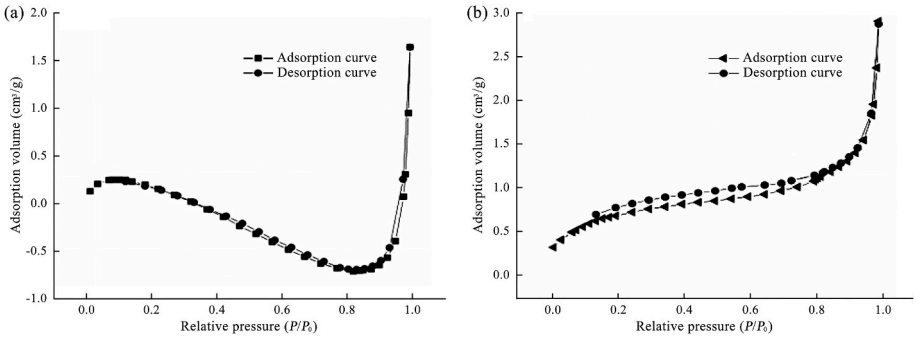

Fig. 1. N_2 adsorption-desorption isotherms of RBIDF (a) and SRBIDF (b).

Table 1
Pore parameters derived from N_2 adsorption data of RBIDF and SRBIDF.

Sample	SSA (m^2/g)	PD (nm)	PV × 10^{-3} (cm^3/g)
RBIDF	0.63 ± 0.02[a]	5.94 ± 0.03[a]	1.13 ± 0.32[a]
S-RBIDF	1.86 ± 0.04[b]	5.38 ± 0.02[b]	3.62 ± 0.41[b]

Mean values with different superscripts (a, b) within the same column indicate a significant difference ($p < 0.05$).

semiconductor sensors, including W1C (aromatic compounds, benzenes), W5S (nitrogen oxides), W3C (aromatic compounds, ammonia), W6S (hydrides), W5C (short-chain alkanes, aromatic components), W1S (methyl compounds, methane), W1W (sulfides), W2S (aldehydes, ketones, alcohols), W2W (sulphur organic compounds, aromatic compounds), W3S (long-chain alkanes). The flavor compounds were extracted from 0.6 g of each sample in a 20 mL headspace vial at 25 °C for 30 min. Subsequently, the headspace gas of the sample was pumped into the sensor chamber at a flow rate of 400 mL/min. The data acquisition time was 60 s and the clean time was 80 s. The sensor data were processed with the software WinMuster PEN 3.5.

2.8. Statistical analysis

All the above measurement experiments were repeated at least three times to acquire mean values and standard deviations, and data were expressed as the mean ± standard deviation. The significance of

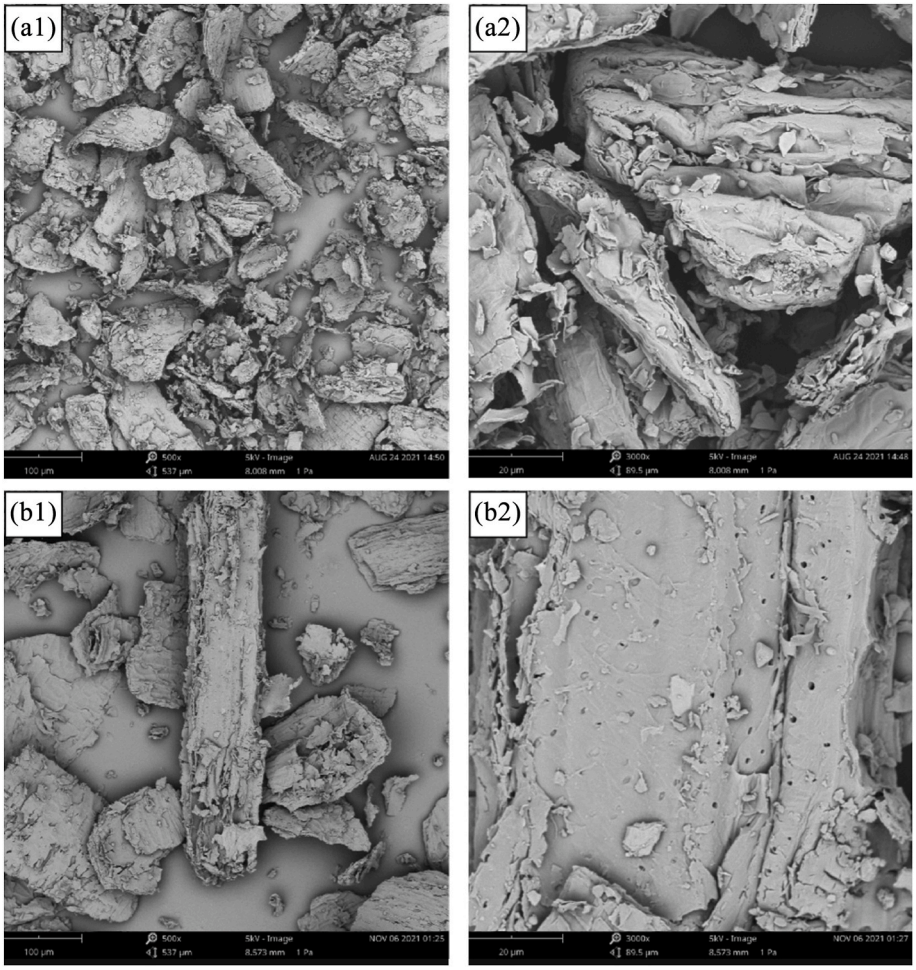

Fig. 2. SEM images of RBIDF under magnifications of 500× (a1) and 3000 × (a2) and SEM images of SRBIDF under magnifications of 500× (b1) and 3000 × (b2).

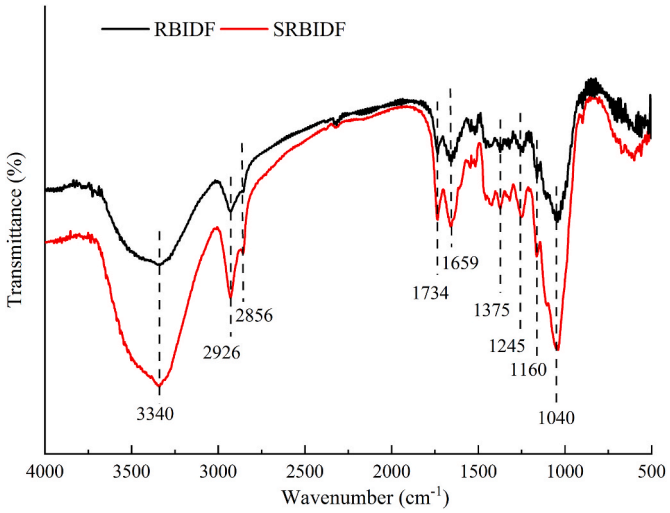

Fig. 3. FT-IR spectra of rice bran insoluble dietary fiber before and after steam explosion treatment.

difference ($p < 0.05$) was analyzed by one-way ANOVA using SPSS 22.0 software. Multiple variable analyses including heatmap analysis of HS-SPME/GC-MS results and principal component analysis (PCA) of E-nose data were conducted using the OriginPro software.

3. Results and discussion

3.1. Changes in the specific area and pore structure of RBIDF before and after steam explosion

The N_2 adsorption/desorption isothermal curves of RBIDF and SRBIDF were shown in Fig. 1. Based on the classification method proposed by International Union of Pure and Applied Chemistry (IPUAC), the adsorption isothermal curve of SRBIDF belonged to type II, showing a convex upward curve shape at low P/P_0 stage, followed by a sharp upward data trend at high P/P_0 stage, which inferred that the adsorption pores of SRBIDF were mainly distributed in mesopores (Tong et al., 2022). It can be seen from the figure that the N_2 adsorption amount on RBIDF was markedly lower than that on SRBIDF in the P/P_0 range 0–0.8. This was likely due to the penetration difficulties of N_2 into the structure of RBIDF. The swelling and unfold characteristics of SRBIDF might facilitate the penetration of N_2 into its structure (Chu et al., 2018).

The hysteresis loop between the adsorption and desorption isotherms can be used for distinguishing the pore shape of the samples (Li et al., 2019). According to classification of IPUAC, the shapes of hysteresis loops of SRBIDF and RBIDF belonged to Type H3, where their desorption curves were almost coincident with the adsorption curves. This indicated that the mesopores of these samples mainly contained slit-like and cylinder pores with good openness (Tong et al., 2022).

The porosity parameters of RBIDF and SRBIDF obtained from N_2 adsorption isothermal curves were shown in Table 1. The estimated SSA and PV of SRBIDF increased by 2.96 times and 3.28 times respectively in comparison with those of RBIDF, which was attributed to that new pores were generated or previously inaccessible pores were opened during steam explosion treatment (Yi et al., 2020). In addition, the PD of SRBIDF decreased by 1.1 times in comparison with that of RBIDF. Previous studies revealed that rice bran had a well-organized structure and readily formed small pores during pyrolysis (Chen et al., 2019). The results indicated that steam explosion treatment also had a positive effect on the pore structure of RBIDF because of the higher SSA and PV values in SRBIDF.

3.2. Structural change of RBIDF before and after steam explosion

The internal structures of RBIDF and SRBIDF were observed by SEM. As shown in Fig. 2, the morphology of RBIDF prior to steam explosion exhibited compact structure with folds. After the steam explosion treatment, the morphology of SRBIDF became loosened, swelling and less folding, the interior fiber was exposed and the increase in surface area and pores was also apparent in the microstructure. These results were consistent with the study of He et al. reporting that steam explosion significantly increased surface area and porosity of the biomass (He et al., 2019). Thus more active sites were exposed during steam explosion, which could improve the adsorption ability of SRBIDF.

FTIR spectra analysis was performed to corroborate chemical changes that happened during the steam explosion. As shown in Fig. 3, all the samples exhibited absorption bands at around 3340, 2926, 2856, 1734, 1659, 1375, 1245, 1160 and 1040 cm^{-1}. The shape and position of the typical peaks of SRBIDF were similar to those of the RBIDF, which indicated that the steam explosion treatment did not change the variety of functional groups of RBIDF, but the intensity of several main peaks changed. Absorption peak at around 3340 cm^{-1} signified –OH stretching vibration in the hydrogen bonds in hemicellulose and cellulose (Liu et al., 2021). The small peaks at 2926 cm^{-1} and 2856 cm^{-1} were associated with the methylene ($–CH_2$) stretching vibrations peaks in sugar ring or branched chain structure (Lv et al., 2019), indicating –CH structure. The peak at around 1734 cm^{-1} was associated with the stretching vibration of C═O group and the peak at around 1659 cm^{-1} was associated with the stretching vibrations of C═C and C–O groups, which indicated the existence of carboxyl group in RBIDF (Zhang et al., 2023). The adsorption peak at 1375 cm^{-1} was associated with the bending vibration of –CH in methyl group (Liu et al., 2021). The weak absorption peak at 1245 cm^{-1} belonged to the stretching vibration of C–O group, while the absorption peaks at 1160 and 1040 cm^{-1} assigned to the stretching vibrations of C–O in glycosidic bond C–O–C and C–O–H on the sugar rings of hemicellulose and cellulose, respectively (Niu et al., 2023). It can be seen from the figure that the peak intensities of some reactive groups (such as hydroxyl bond, carbonyl, ester and ether groups) of SRBIDF were higher than those of RBIDF. This might be due to the fact that steam explosion treatment caused the structure of

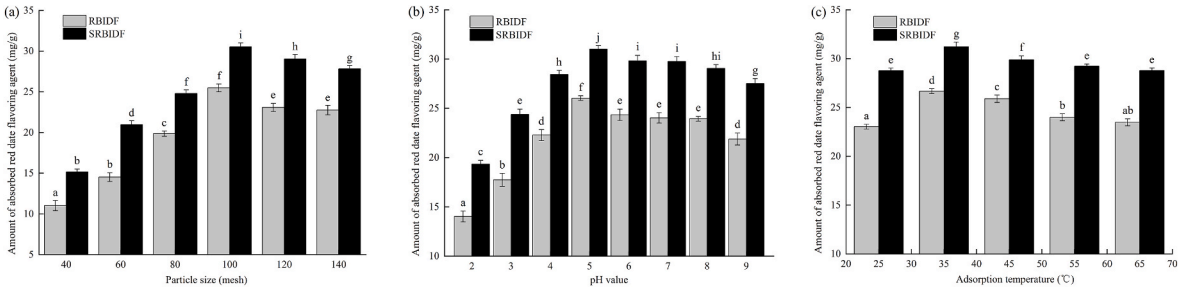

Fig. 4. Adsorption capacity of red date flavoring agent by RBIDF and SRBIDF with different particle sizes (a), at different pH values (b) and temperatures (c). Different letters (a–i) indicated significant difference ($p < 0.05$).

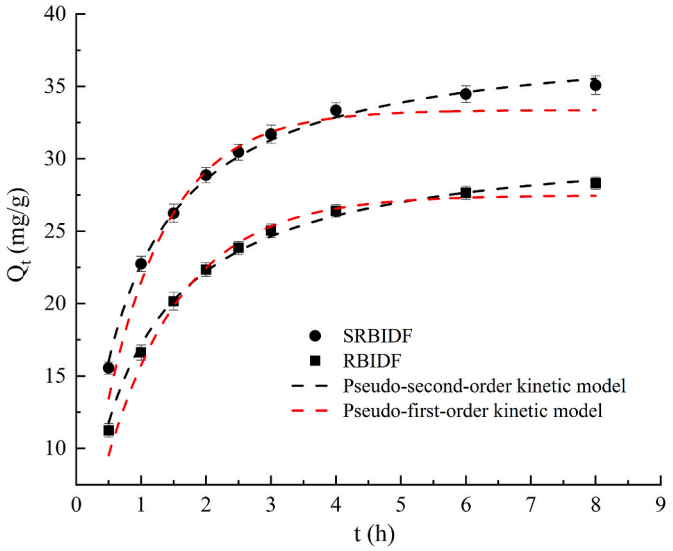

Fig. 5. Adsorption kinetics of red date flavoring agent on RBIDF and SRBIDF.

cellulose to loosen, causing more free functional groups to become exposed, which aided in the adsorption and retention of flavor compounds on RBIDF.

3.3. Flavor adsorption property of RBIDF before and after steam explosion

3.3.1. Effect of different factors on flavor adsorption onto RBIDF

The adsorption experiments of red date flavoring agent by RBIDF and SRBIDF were carried out as a function of pH, temperature and adsorbent particle size. As shown in Fig. 4a, the adsorption capacity of red date flavoring agent by RBIDF and SRBIDF increased with the decrease in the adsorbent particle size, and reached the largest level when the adsorbent particle size was 100 mesh. This might be attributed to the fact that with the decrease in absorbent particle size, the surface area of absorbent expanded and more adsorption active sites were present on the absorbent surface (Yi et al., 2020). In addition, the adsorption capacity per gram was found to close to the equilibrium state when the absorbent particle size exceeded 100 mesh. The reason might be that smaller particle size reduced the permeability of the absorbent, thus increasing the flow resistance through the voids (Zhou et al., 2023).

The adsorption capacity of red date flavoring agent by RBIDF and SRBIDF at different pH value was shown in Fig. 4b. The adsorption capacity increased as the pH value increased from 2 to 5, exhibited maximum value at pH = 5, and then gradually decreased at the pH higher than 5. The solution pH can affect the surface property of adsorbent as well as adsorbate which in turn will affect the adsorption capacity (Bayrac et al., 2022). According to above testing results, at pH higher than 5, the dominance of OH^- ions in the solution repelled the contact between the adsorbent and adsorbate, or create a competition between adsorbent surface and OH^- ions (Yadav and Dasgupta, 2022), which diminished adsorption of red date flavoring agent onto the absorbent.

Temperature is also an important factor that may affect adsorption of red date flavoring agent by affecting molecular interactions with solid particles (Wang et al., 2022). The adsorption capacity of red date flavoring agent by RBIDF and SRBIDF at different temperature was shown in Fig. 4c. It can be seen that the adsorption capacity of red date flavoring agent increased as the temperature increased up to 35 °C, which might be due to the possibility of increase in the rate and mobility of diffusion of red date flavoring agent into the interlayer space of absorbents (Zhou et al., 2023). The observed decrease in the adsorption of red date flavoring agent at further high temperature was probably due to the decrease in bonding affinity between the adsorbate and the active sites on the surface of adsorbents (Yadav and Dasgupta, 2022). Based on the results it seems that the maximum adsorption capacities of red date flavoring agent onto RBIDF and SRBIDF were obtained at pH 5, temperature 35 °C and absorbent particle size 100 mesh.

Table 2
Fitted parameters and correlation coefficients (R^2) of pseudo first order and pseudo second order models on the adsorption of red date flavoring agent by RBIDF and SRBIDF.

Models	Parameters	Samples	
		RBIDF	SRBIDF
	Experimental Q_e (mg/g)	28.07 ± 0.53[a]	35.12 ± 0.62[b]
Pseudo-first-order	Calculated k_1 (min^{-1})	0.85 ± 0.02[a]	1.12 ± 0.05[b]
	Calculated Q_e (mg/g)	27.48 ± 0.49[a]	33.67 ± 0.55[b]
	R^2	0.9817	0.9830
Pseudo-second-order	Calculated k_2 (g/(mg·h))	0.0379 ± 0.0008[a]	0.0415 ± 0.0012[b]
	Calculated Q_e (mg/g)	28.64 ± 0.51[a]	36.46 ± 0.95[b]
	R^2	0.9914	0.9972

Mean values with different superscripts (a, b) in the same row differ significantly ($p < 0.05$).

3.3.2. Adsorption kinetics

To examine the adsorption kinetics of red date flavoring agent on RBIDF and SRBIDF, pseudo-first-order and pseudo-second-order models were applied to fit the adsorption experimental curves. The fitting results were shown in Fig. 5. It can be observed that the adsorption amount of red date flavoring agent onto RBIDF and SRBIDF increased rapidly in the initial stage, and then the adsorption slowed down at about 4 h. This can be due to a large number of vacant binding sites present on the adsorbent surface at the early stage. When these adsorption sites available were occupied, no more adsorption reaction happened (Chen et al., 2021). The adsorption kinetics parameters calculated from the two models are listed in Table 2. It can be observed that the correlation coefficients of pseudo-second-order model (R^2 = 0.9972 and 0.9914) were higher than those of the pseudo-first-order model (R^2 = 0.9830 and 0.9817), and the calculated Q_e values from pseudo-second-order model were closer to the experimental Q_e values compared to those from pseudo-first order model, indicating that the adsorption experiment data for RBIDF and SRBIDF were better fitted by the pseudo-second-order

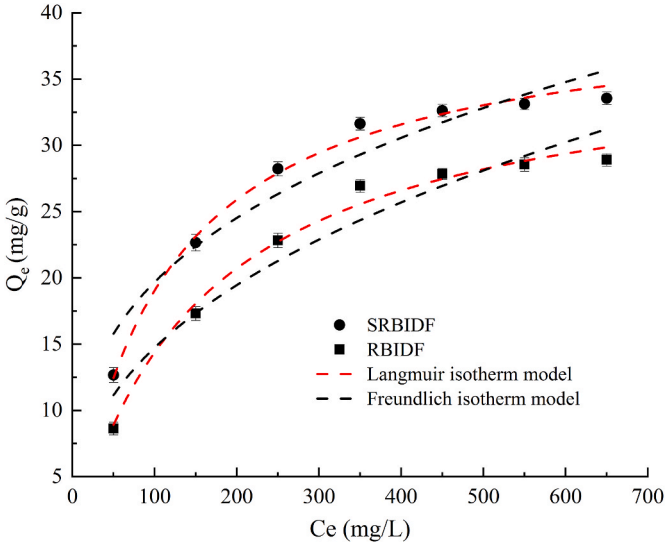

Fig. 6. Adsorption isotherms for the adsorption of red date flavoring agent onto RBIDF and SRBIDF.

Table 3
Fitted parameters and correlation coefficients (R^2) of Langmuir and Freundlich isotherm models on the adsorption of red date flavoring agent by RBIDF and SRBIDF.

Models	Parameters	Samples	
		RBIDF	SRBIDF
Langmuir model	Q_{max} (mg/g)	31.82 ± 0.83[a]	38.45 ± 0.94[b]
	K_L (L/mg)	0.0065 ± 0.0002[a]	0.0089 ± 0.0003[b]
	R^2	0.9872	0.9805
Freundlich model	K_f ((mg/g)/(L/mg)$^{1/n}$)	2.32 ± 0.07[a]	4.55 ± 0.05[b]
	1/n	0.41 ± 0.01[a]	0.32 ± 0.01[b]
	R^2	0.9231	0.9089

Mean values with different superscripts (a, b) in the same row differ significantly ($p < 0.05$).

Table 4
Thermoanalytical data for RBIDF and SRBIDF before and after the adsorption of red date flavoring agent.

Samples	T_{p1} (°C)	ΔH_1 (J/g)	T_{p2} (°C)	ΔH_2 (J/g)
RBIDF before adsorption	94.86 ± 1.21[a]	125.45 ± 2.31[a]	–	–
SRBIDF before adsorption	109.43 ± 2.41[b]	187.63 ± 1.94[b]	–	–
RBIDF after adsorption	108.26 ± 2.26[b]	106.78 ± 1.65[c]	175.35 ± 1.15[a]	78.74 ± 1.34[a]
SRBIDF after adsorption	107.15 ± 1.43[b]	106.24 ± 2.17[c]	175.76 ± 1.21[a]	85.55 ± 2.02[b]

Mean values with different superscripts within the same column differ significantly ($p < 0.05$). T_{p1}: peak temperature corresponding to free or bound water evaporation; T_{p2}: peak temperature corresponding to decomposition of red date flavor essence; ΔH_1: Enthalpy of bound water evaporation; ΔH_2: Enthalpy of red date flavoring agent decomposition; —: Not determined.

model. Pseudo-first-order model generally assumes that physical sorption is the rate-determine step, and the adsorption capacity is a proportion to the number of unoccupied adsorption sites. While pseudo-second-order kinetic model assumes that the adsorption involves strong chemisorption (Chen et al., 2021). The results indicated that the retention of red date flavoring agent on RBIDF and SRBIDF was mainly driven by chemical interactions between the red date flavoring agent and the surface functional groups (such as hydroxyl, carboxyl and aldehyde groups) in the adsorbents. In addition, the correlation coefficients of pseudo-first-order model were higher than 0.95, so the pseudo-first-order equation was also applicable to the adsorption process. These observations indicated that the adsorption of red date flavoring agent on RBIDF and SRBIDF involved both chemical and physical adsorption processes, but the facilitation for chemisorption was possibly more than for physisorption.

3.3.3. Adsorption isotherm

Adsorption isotherm analysis could give an insight into the adsorption mechanism of red date flavoring agent by RBIDF and SRBIDF and the affinity of adsorbate towards adsorbents. Fig. 6 showed the isotherms of red date flavoring agent adsorbed on RBIDF and SRBIDF. The adsorption capacities increased with the increase in the initial concentration of red date flavoring agent. However, at higher initial concentration, the adsorption capacities reached equilibrium as the number of binding sites available on the surface of the absorbents decreased. The fitted parameters and correlation coefficient values (R^2) for Langmuir and Freundlich isotherm models were shown in Table 3. The parameter 1/n reflected adsorption intensity, and the 1/n value in the range of 0.1–0.5 implied that adsorption of red date flavoring agent on the adsorbent was favorable (Wu et al., 2021b). Besides, the 1/n value of SRBIDF was lower than that of RBIDF, indicating that SRBIDF had higher adsorption intensity and affinity for red date flavoring agent than RBIDF (Khamwichit et al., 2022). In addition, it can be observed that the correlation coefficients of Langmuir model (R^2 = 0.9872 and 0.9805) were higher than those of the Freundlich model (R^2 = 0.9231 and 0.9089), indicating that the equilibrium adsorption of red date flavoring agent on RBIDF and SRBIDF could be better described by Langmuir model. The Langmuir isotherm is based on monolayer adsorption on a homogeneous surface and it is considered that the active sites on the adsorbent surface are equally probable for the adsorption (Yadav and Dasgupta, 2022). The results indicated that red date flavoring agent can be adsorbed in the form of monolayer and homogeneous adsorption on the surface of the absorbents. The maximum adsorption capacity of red date flavoring agent on RBIDF and SRBIDF determined by Langmuir isotherm was found to be 31.32 and 38.45 mg/g, respectively.

3.3.4. The structure properties of RBIDF and SRBIDF after flavor adsorption

The thermal transformation of RBIDF and SRBIDF before and after adsorption the of red date flavoring agent was analyzed using DSC. The DSC curve of pure red date flavoring agent showed endothermic peaks at 161.51 °C and 210.43 °C, respectively (Fig. 7). They were assigned to the thermal decomposition and carbonization process of red date flavoring agent, respectively (Rezaeinia et al., 2020). The DSC curves of RBIDF and SRBIDF samples showed a broad endothermic peak at 90–110 °C, which could be attributed to loss of free or bound water present in the insoluble dietary fiber (Ouyang et al., 2023b). The details of thermal effect peak data including peak temperature (T_{p1}) and enthalpy of bound water evaporation (ΔH_1) obtained from DSC determinations were shown in Table 4. It can be seen that before adsorption of red date flavoring agent, SRBIDF had a higher ΔH_1 than RBIDF, and the endothermic peak of SRBIDF shifted to a higher temperature compared with RBIDF. These phenomena might be due to the fact that steam explosion treatment increased the exposure of the functional groups such as hydrogen bonds, leading to an increased content of bound water. After the adsorption of red date flavoring agent, the DSC

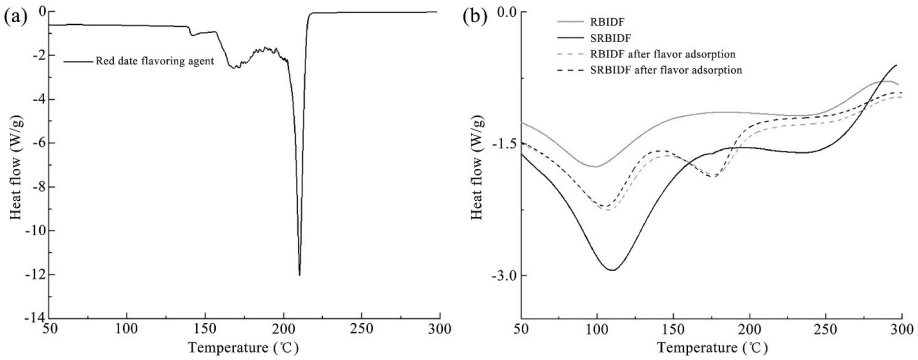

Fig. 7. DSC curves of RBIDF and SRBIDF before and after the adsorption of red date flavoring agent.

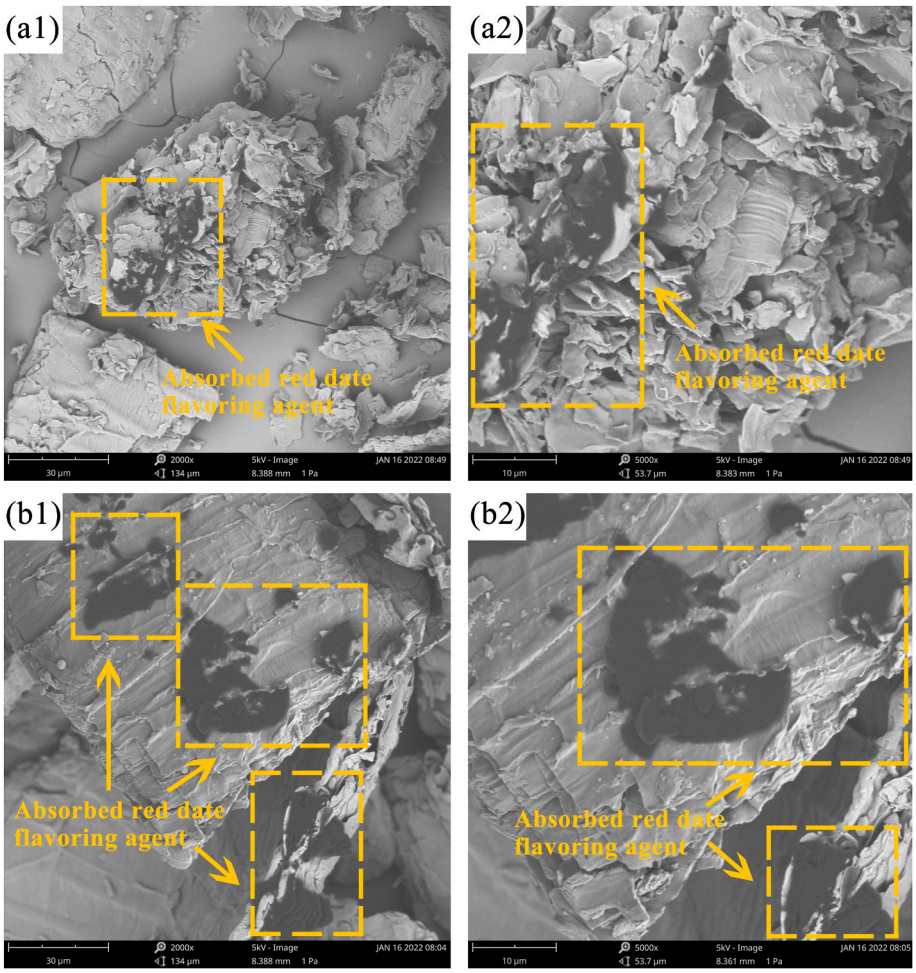

Fig. 8. SEM images of RBIDF (a1, a2) and SRBIDF (b1, b2) at magnifications of × 2000 (a1, b1) and × 5000 (a2, b2) after the adsorption of red date flavoring agent.

curves of RBIDF and SRBIDF showed a new endothermic peak at 175.35 °C and 175.76 °C respectively, which were attributed to the thermal decomposition of red date flavoring agent in the absorbents. In addition, the temperature of this peak (T_{p2}) of RBIDF and SRBIDF was higher than the decomposition temperature of pure red date flavoring agent (161.51 °C), indicating that these flavor compounds were retained in RBIDF and SRBIDF absorbents above their decomposition temperature, implying an improvement in their thermal stability, this result was consistent with the work of Ishii et al. (2006) for the flavor adsorption of clay mineral. The endothermic enthalpy of red date flavoring agent decomposition (ΔH_2) was shown in Table 1. SRBIDF had a higher ΔH_2 value than RBIDF after the adsorption of red date flavoring agent, indicating that the evaporation and decomposition of red date flavoring agent absorbed in SRBIDF required relatively higher energetics. This might be related to the ability of SRBIDF to retain the flavor compounds (Ishii et al., 2006).

SEM was employed to observe the surface morphology of RBIDF and SRBIDF absorbents before and after adsorption of red date flavoring agent. It can be seen from Fig. 8 that after the adsorption of red date flavoring agent, some black carbon-like particles were distributed uniformly on the holes and surface of the absorbents. Compared with RBIDF, the amount of red date flavoring agent absorbed on the surface of SRBIDF was relatively higher. The loose and large surface area characteristics of SRBIDF were beneficial for binding flavor compounds because of the exposure of more active sites.

3.4. Analysis of the flavor release characteristics from RBIDF before and after steam explosion via HS-SPME GC/MS

3.4.1. Flavor characteristics of red date flavoring agent

The individual volatile profiles of red date flavoring agent were summarized in Table 5. A total of 18 flavor compounds were identified in red date flavoring agent, including 7 esters, 3 phenols, 3 ketones, 3 alcohols and 2 aldehydes. Specifically, it can be seen that the concentrations of the top ten volatile compounds were in the decreasing order of ethyl maltol (2999.73 μg/kg), trans-cinnamaldehyde (1634.76 μg/kg), benzyl butyrate (1291.39 μg/kg), citronellate acetate (556.55 μg/kg), methylcyclopentanol ketone (509.39 μg/kg), *β*-damarone (386.76 μg/kg), ethanol (347.14 μg/kg), dimethyl phthalate (338.89 μg/kg), benzyl alcohol (316.95 μg/kg), 2-hydroxypropyl acetate (94.33 μg/kg). The contribution of volatile compounds to red date flavoring agent was not only related to the concentration, but also to the threshold value. The OAV value of each flavor component was calculated based on the concentrations in Table 4. There were 10 flavor compounds with OAV values higher than 1, indicated that they were the main key aroma compounds in the sample. Among these aroma components, there were two compounds with OAV values higher than 1000, including *β*-damarone and *β*-lonone, which contributed to the fruity and floral flavor in red date flavoring agent. Four compounds with OAV values ranging from 10 to 1000, including ethyl acetate, benzyl alcohol, trans-cinnamaldehyde and ethyl maltol, contributed to the flavor of fruity, roasty and caramel. Four compounds with OAV values ranging from 1 to 10, including isoamyl isovalerate, methylcyclopentanol ketone, vanilla, and engenol, contributed to the fruity, caramel and smoky odor.

Table 5
The flavor compounds and their concentrations of red date flavoring agent identified by GC-MS.

No	Retention time (min)	Molecular formular	Calculated RI	Literature RI	Qualitative method	Volatile compound	Odor description	Concentration (μg/kg)	Odor threshold (μg/kg)	OAV
1	2.82	$C_4H_8O_2$	638	645	MS, RI, Std	Ethyl acetate	Fruity aroma	83.95 ± 0.22	5	16.790
2	13.16	$C_{10}H_{20}O_2$	1104	1109	MS, RI, Std	Isoamyl isovalerate	Apple fragrance	23.58 ± 0.16	3	7.860
3	20.74	$C_5H_{10}O_3$	883	892	MS, RI	2-hydroxypropyl acetate	–	94.33 ± 0.17	–	–
4	22.64	$C_{12}H_{22}O_2$	1354	1353	MS, RI, Std	Citronellate acetate	Herbal fragrance	556.55 ± 0.26	1000	0.056
5	25.68	$C_{14}H_{26}O_2$	1483	–	MS, RI, Std	Citronellyl isobutyrate	Rose aroma	34.9 ± 0.08	–	–
6	27.18	$C_{11}H_{14}O_2$	1345	1355	MS, RI, Std	Benzyl butyrate	Light floral aroma of jasmine fragrance, pineapple aroma	1291.39 ± 0.19	–	–
7	32.73	$C_{10}H_{10}O_4$	1454	1445	MS, RI	Dimethyl phthalate	Sweet aroma	338.89 ± 0.08	–	–
8	26.03	$C_{13}H_{20}O$	1417	1429	MS, RI, Std	*β*-damarone	Honey aroma, floral aroma	386.76 ± 0.17	0.002	193380
9	26.50	$C_6H_8O_2$	1034	1027	MS, RI	Methylcyclopentanol ketone	Maple aroma, sweet caramel aroma	509.39 ± 0.09	300	1.698
10	28.24	$C_{13}H_{20}O$	1491	1483	MS, RI, Std	*β*- lonone	Floral aroma of violet, fruity aroma	73.58 ± 0.18	0.007	10511
11	3.5	$C_2H_6O_2$	427	442	MS, RI, Std	Ethanol	Alcohol fragrance	347.14 ± 0.20	100000	0.003
12	25.07	$C_{10}H_{20}O$	1228	1226	MS, RI, Std	Citronellol	Rose aroma, sweet aroma	7.55 ± 0.21	40	0.180
13	27.40	C_7H_8O	1036	1031	MS, RI, Std	Benzyl alcohol	Sweet aroma, roasted aroma	316.95 ± 0.07	20	15.847
14	19.36	C_7H_6O	962	957	MS, RI	Benzaldehyde	Almond fragrance	17.92 ± 0.25	350	0.051
15	29.81	C_9H_8O	1274	1266	MS, RI, Std	Trans-cinnamaldehyde	Cinnamon fragrance, light fruity aroma,	1634.76 ± 0.43	53	30.844
16	28.79	$C_6H_6O_3$	1110	1115	MS, RI	Methyl maltol	Sweet caramel aroma	78.29 ± 0.11	35000	0.002
17	29.51	$C_7H_8O_3$	1199	1212	MS, RI, Std	Ethyl maltol	Caramel aroma	2999.73 ± 0.12	44	68.175
18	31.35	$C_{10}H_{12}O_2$	1357	1354	MS, RI, Std	Eugenol	Smoky fragrance, smoked meat aroma	11.32 ± 0.18	7.1	1.594

Literature RI values were from NIST MS Search 2.3 database.
Qualitative method: Std, confirmed by authentic standards; MS, mass spectrum comparison; RI, agreed with the published retention indices.
Odor thresholds in water/air were obtained from literature (Van Gemert, 2011).
Odor descriptions were obtained from literatures (Niu et al., 2021; Pino and Mesa, 2006; Song et al., 2020; Sun and Chen, 2017; Sun et al., 2000; Xu et al., 2019).
—: No information was found in the literature.

3.4.2. Controlled release of flavor compounds from RBIDF and SRBIDF during storage

The individual volatile profiles of RBIDF and SRBIDF after flavor adsorption were listed in Table 6. A total of 21 flavor compounds were detected from the headspace volatiles of RBIDF and SRBIDF, among which 10 flavor substances of red date flavoring agent were detected in RBIDF, while 13 were detected in SRBIDF. These red date flavor substances included benzaldehyde, benzyl alcohol, trans-cinnamaldehyde, citronellol, methyl maltol, ethyl maltol, engenol, *β*-damarone, methylcyclopentanol ketone, *β*-lonone, benzyl butyrate, dimethyl phthalate, 2-hydroxypropyl acetate. The rest of the flavor substances are considered as endogenous to rice bran, and they had no significant effect the overall flavor profile due to their low concentrations. Among the aldehydes identified, trans-cinnamaldehyde showed the highest concentration in RBIDF and SRBIDF samples. The concentration of trans-cinnamaldehyde decreased from 9.19 μg/kg to 1.08 μg/kg in RBIDF after 28 days of storage, while in SRBIDF, this value decreased from 14.96 μg/kg to 4.42 μg/kg. Among the alcohols identified, the concentration of benzyl alcohol was the highest, which decreased from 17.43 μg/kg to 1.08 μg/kg in RBIDF sample after 28 days, while in SRBIDF, the concentration of benzyl alcohol decreased from 23.77 μg/kg to 6.84 μg/kg. Among the phenols, the concentration of ethyl maltol was the highest, which decreased from 31.04 μg/kg to 2.07 μg/kg after 28 days, while in SRBIDF, this value decreased from 83.09 μg/kg to17.04 μg/kg. Methylcyclopentanol ketone, *β*-damascenon, benzyl butyrate and dimethyl phthalate were the most abundant ketone and ester compounds in the samples, and the concentrations of these substances were higher in SRBIDF than those in RBIDF during storage. These results indicated that the release amount of red date flavor compounds in SRBIDF was higher than that in RBIDF during 28 days of storage, which might be due to the higher retention ability and controlled release capacity of SRBIDF for the flavor compounds. Results of conformation analysis showed that steam explosion treatment significantly altered the degree of swelling and unfolding, the specific surface area and the porosity of RBIDF (Table 1 and Fig. 2). The unfolding structure and increased surface area of SRBIDF resulted in the exposure of more interior flavor bind sites. The increase in the porosity and binding sites inhibited flavor molecules to diffuse in the interlayer space, thus contributing to the retention and sustained release of volatile compounds (Xu et al., 2022).

Fig. 9 was a clustering heatmap of the 13 red date flavor compounds in RBIDF and SRBIDF at different storage time. The heatmap exhibited the concentrations of the red date flavor compounds in each sample by different colors. It can be seen that the concentrations of red date flavor compounds in RBIDF and SRBIDF samples showed gradually decreasing trend due to their release into the air during storage. The colors of the heat map of SRBIDF sample between day 0 and day 14 were largely white and red, indicating that most red date flavor compounds in the samples were high in concentration. According to the cluster tree of samples constructed on the upper side (Fig. 9), all the samples were clustered into three clusters: The first cluster was composed of RBIDF samples at day 0, day 7, day 14, day 21 and day 28 and SRBIDF samples at day 21 and day 28. The second cluster was composed of SRBIDF

Table 6
Comparison of the released flavor compounds from RBIDF and SRBIDF during storage.

	No	Qualitative method	Volatile compound	Concentration (μg/kg)									
				RBIDF					S-RBIDF				
				0 d	7 d	14 d	21 d	28 d	0 d	7 d	14 d	21 d	28 d
Aldehydes	1	MS, RI	Benzaldehyde※	2.95 ± 0.03^{a}	2.55 ± 0.07^{b}	2.46 ± 0.03^{b}	1.66 ± 0.03^{c}	1.32 ± 0.01^{d}	3.15 ± 0.08^{e}	2.14 ± 0.05^{f}	2.54 ± 0.07^{b}	2.07 ± 0.04^{f}	1.37 ± 0.06^{d}
	2	MS, RI, Std	Trans-cinnamaldehyde※	9.19 ± 0.12^{a}	8.66 ± 0.08^{b}	7.11 ± 0.06^{c}	6.10 ± 0.07^{d}	1.08 ± 0.02^{e}	14.96 ± 0.02^{f}	12.63 ± 0.03^{g}	8.95 ± 0.05^{h}	5.55 ± 0.14^{i}	4.42 ± 0.09^{j}
	3	MS, RI	(E)-2-hepteneal	0.25 ± 0.03^{a}	0.18 ± 0.02^{b}	0.12 ± 0.02^{c}	–	–	–	0.23 ± 0.02^{a}	0.16 ± 0.01^{b,c}	0.12 ± 0.02^{c}	–
	4	MS, RI, Std	Nonanal	0.37 ± 0.06^{a,b}	0.33 ± 0.02^{b,c}	0.29 ± 0.04^{c,d}	0.36 ± 0.02^{a,b}	0.41 ± 0.01^{a}	0.28 ± 0.03^{c,d}	0.26 ± 0.02^{d,e}	0.21 ± 0.02^{e,f}	0.16 ± 0.01^{f}	0.22 ± 0.02^{e,f}
	5	MS, RI, Std	Decanal	0.34 ± 0.02^{a}	0.31 ± 0.02^{a,b}	0.25 ± 0.03^{c,d}	0.24 ± 0.01^{d}	0.19 ± 0.01^{e}	0.29 ± 0.02^{b,c}	0.27 ± 0.03^{b,c,d}	0.23 ± 0.02^{d}	0.17 ± 0.01^{e}	0.12 ± 0.01^{f}
Alcohols	6	MS, RI, Std	Citronellol※	–	–	–	–	–	0.61 ± 0.04^{a}	–	–	–	–
	7	MS, RI, Std	Benzyl alcohol※	17.43 ± 0.22^{a}	17.02 ± 0.15^{b}	16.52 ± 0.15^{c}	14.8 ± 0.06^{d}	3.02 ± 0.06^{e}	23.77 ± 0.11^{f}	22.73 ± 0.13^{g}	18.88 ± 0.08^{h}	13.37 ± 0.11^{i}	6.84 ± 0.11^{j}
	8	MS, RI, Std	2-ethylhexanol	0.33 ± 0.02^{a,b}	0.28 ± 0.03^{b,c}	0.17 ± 0.02^{e}	0.24 ± 0.03^{c,d}	0.29 ± 0.02^{b,c}	0.36 ± 0.03^{a}	0.21 ± 0.02^{d}	0.13 ± 0.01^{e}	0.14 ± 0.02^{e}	0.28 ± 0.02^{b,c}
	9	MS, RI, Std	N-octanol	0.22 ± 0.02^{a}	0.15 ± 0.01^{b,c}	0.18 ± 0.01^{a,b}	0.21 ± 0.02^{a}	0.19 ± 0.03^{a}	0.21 ± 0.02^{a}	0.11 ± 0.01^{d}	0.08 ± 0.01^{e}	0.13 ± 0.01^{c,d}	0.18 ± 0.02^{a,b}
Phenols	10	MS, RI	Methyl maltol※	0.49 ± 0.07^{a,b}	0.57 ± 0.05^{a}	0.45 ± 0.04^{b}	0.34 ± 0.01^{c}	–	1.22 ± 0.02^{d}	1.4 ± 0.06^{e}	0.9 ± 0.08^{f}	0.57 ± 0.02^{a}	0.33 ± 0.05^{c}
	11	MS, RI, Std	Ethyl maltol※	31.85 ± 0.14^{a}	31.04 ± 0.12^{b}	27.82 ± 0.15^{c}	14.73 ± 0.11^{d}	2.07 ± 0.13^{e}	83.09 ± 0.21^{f}	78.87 ± 0.17^{g}	60.83 ± 0.14^{h}	34.50 ± 0.22^{i}	17.04 ± 0.15^{j}
	12	MS, RI, Std	Engenol※	–	–	–	–	–	0.7 ± 0.03^{a}	0.47 ± 0.02^{b}	0.36 ± 0.04^{c}	–	–
	13	MS, RI, Std	2,6-di-tert-butyl-4-methylphenol	0.27 ± 0.02^{a}	0.20 ± 0.03^{b}	0.16 ± 0.01^{b,c}	0.13 ± 0.01^{c}	–	0.36 ± 0.03^{d}	0.29 ± 0.02^{a}	0.26 ± 0.01^{a}	0.18 ± 0.02^{b}	0.16 ± 0.01^{b,c}
Ketones	14	MS, RI, Std	*β*-damarone※	1.16 ± 0.08^{a,b}	1.08 ± 0.03^{b}	0.92 ± 0.02^{c}	0.77 ± 0.02^{d,e}	0.33 ± 0.01^{f}	1.88 ± 0.06^{g}	1.26 ± 0.05^{a}	1.20 ± 0.03^{a}	0.85 ± 0.07^{c,d}	0.72 ± 0.08^{e}
	15	MS, RI	Methylcyclopentanol ketone※	6.72 ± 0.07^{a}	6.54 ± 0.09^{b}	6.44 ± 0.04^{b}	5.84 ± 0.03^{c}	0.65 ± 0.02^{d}	15.85 ± 0.14^{e}	15.73 ± 0.09^{e}	9.9 ± 0.07^{f}	8.29 ± 0.05^{g}	2.38 ± 0.12^{h}
	16	MS, RI, Std	*β*-lonone※	0.53 ± 0.05^{a}	0.57 ± 0.04^{a}	0.42 ± 0.02^{b}	0.57 ± 0.02^{a}	0.11 ± 0.01^{c}	1.65 ± 0.05^{d}	1.13 ± 0.02^{e}	0.79 ± 0.06^{f}	0.52 ± 0.04^{a}	0.36 ± 0.04^{b}
Esters	17	MS, RI, Std	Benzyl butyrate※	1.42 ± 0.05^{a}	1.21 ± 0.09^{b}	1.24 ± 0.05^{b}	2.20 ± 0.03^{c}	1.36 ± 0.02^{a}	2.32 ± 0.03^{d}	1.61 ± 0.01^{e}	1.55 ± 0.13^{e}	0.83 ± 0.03^{f}	1.04 ± 0.05^{g}
	18	MS, RI	Dimethyl phthalate※	1.91 ± 0.08^{a}	1.13 ± 0.03^{b}	1.53 ± 0.06^{c}	1.07 ± 0.02^{b}	0.56 ± 0.02^{d}	2.49 ± 0.06^{e}	2.16 ± 0.08^{f}	1.91 ± 0.02^{a}	0.72 ± 0.03^{g}	0.82 ± 0.07^{h}
	19	MS, RI	2-hydroxypropyl acetate※	–	–	–	–	–	3.14 ± 0.34^{a}	1.74 ± 0.26^{b}	–	–	–
	20	MS, RI, Std	Methyl propionate	0.38 ± 0.03^{a}	–	0.23 ± 0.03^{b}	0.29 ± 0.02^{c}	–	0.22 ± 0.03^{b}	0.25 ± 0.02^{b,c}	0.16 ± 0.02^{d}	0.14 ± 0.01^{d}	0.09 ± 0.02^{e}
Furans	21	MS, RI	2-pentylfuran	0.15 ± 0.01^{a}	0.22 ± 0.02^{b}	0.26 ± 0.04^{b,c}	0.28 ± 0.01^{b,c}	0.31 ± 0.03^{c}	0.14 ± 0.02^{a}	0.17 ± 0.02^{a}	0.23 ± 0.03^{b}	0.26 ± 0.02^{b,c}	0.25 ± 0.03^{b,c}

Mean values with different superscripts (a-j) in the same row differs significantly ($p < 0.05$).
—: not determined.
※: volatiles derived from the red date flavor essence.
Qualitative method: Std, confirmed by authentic standards; MS, mass spetrum comparison; RI, agreed with the published retention indices.

samples at day 7 and day 14. The SRBIDF sample at day 0 was counted as the third cluster. Results of the cluster analysis showed that the concentrations of red date flavor compounds of SRBIDF at day 0, day 7 and day 14 were significantly different from those of RBIDF, indicating that the flavor compounds were retained at higher concentrations in SRBIDF than in RBIDF during storage. This might be due to the fact that SRBIDF had a higher sustained flavor release ability compared to RBIDF. As the storage proceeded, the release rate of SRBIDF gradually decreased. It can be observed that the RBIDF and SRBIDF samples at day 28 were clustered into the same cluster (Fig. 9).

Fig. 10 reflected the differences of concentrations and varieties of red date flavor compounds in RBIDF and SRBIDF samples at different storage time. Phenols and alcohols were the two dominant red date flavor compounds in RBIDF and SRBIDF, accounting for more than 50% and 15% of the total red date flavor compounds in the samples, respectively. The contents of phenols and alcohols of SRBIDF were enhanced by 1.6 fold and 0.4 fold in comparison with those of RBIDF respectively. Aldehydes, ketones and esters accounted for more than 10%, 11% and 4% of the total red date flavor compounds in the samples respectively, and it can be observed thatthe contents of aldehydes, ketones and esters in SRBIDF were enhanced by 1.5 fold, 0.6 fold and 2.1 fold respectively, in comparison with those in RBIDF. Besides, the number of phenol, alcohol and ester compounds in SRBIDF were higher than those in RBIDF during storage. Eugenol, 2-hydroxypropyl acetate and citronellol that were not detected in RBIDF were detected SRBIDF. Phenols and alcohols contained hydroxyl and phenolic hydroxyl groups, and they could bind to the rice bran dietary fiber via intermolecular hydrogen bonding interactions. Aldehydes, ketones and esters compounds could bind to the dietary fiber via hydrophobic interactions (Ullah et al., 2023). Results indicated that the swelling and unfolding of SRBIDF after steam explosion treatment resulted in the exposure of more hydrophilic and hydrophobic functional groups (such as hydroxyl groups, carbonyl, ester and ether groups, etc.), which could form more intermolecular interactions and thus improve the retention and controlled release

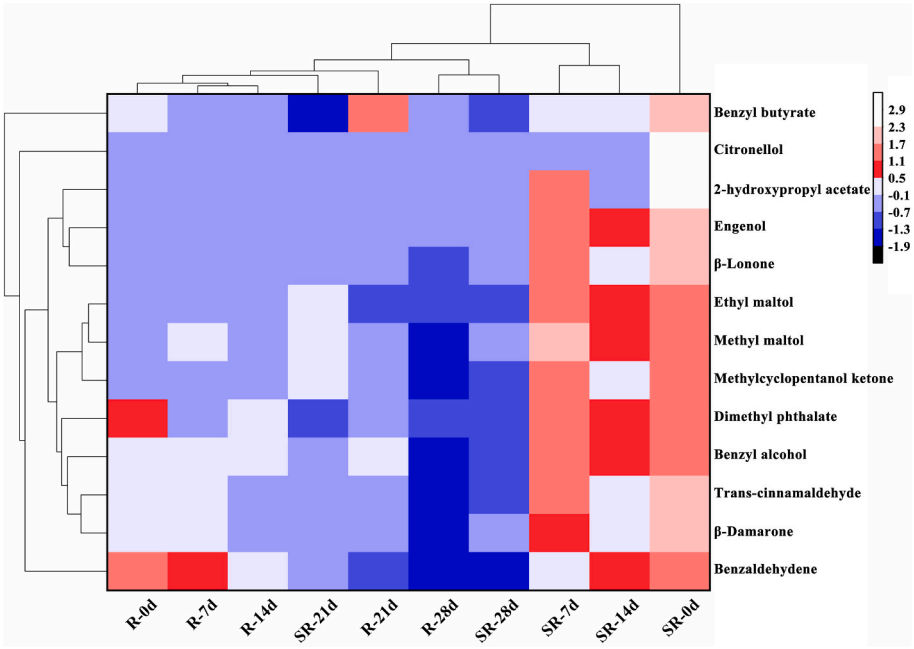

Fig. 9. Heat map and clustering results of red date flavor compounds in SRBIDF and RBIDF during storage. R-0d, R-7d, R-14 d, R-21 d, R-28 d represented the RBIDF samples stored for 0, 7, 14, 21, and 28 days, respectively; RS-0d, RS-7d, RS-14 d, RS-21 d, RS-28 d represented the SRBIDF samples stored for 0, 7, 14, 21, and 28 days, respectively.

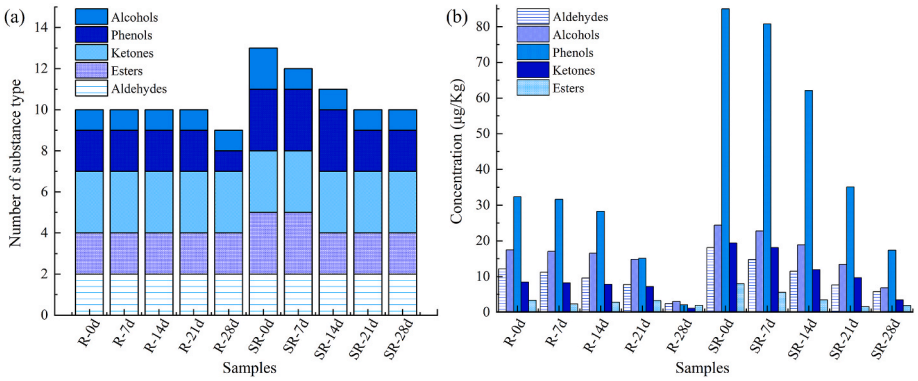

Fig. 10. The number of types (a) and the total concentration for each type (b) of red date flavor compounds released from SRBIDF and RBIDF. R-0d, R-7d, R-14 d, R-21 d, R-28 d represented the RBIDF samples stored for 0, 7, 14, 21, and 28 days, respectively; RS-0d, RS-7d, RS-14 d, RS-21 d, RS-28 d represented the SRBIDF samples stored for 0, 7, 14, 21, and 28 days, respectively.

capacities of SRBIDF for these flavor compounds. In addition, results showed that the SRBIDF sample had a higher retention capacity for polar volatile compounds (such as alcohols and phenols) than for non-polar volatile compounds (such as aldehydes, ketones and esters), indicating higher content of hydrophilic groups on the surface of SRBIDF after steam explosion treatment.

3.5. Analysis of the flavor release characteristics from RBIDF via E-nose

The E-nose, similar to the human nose, was used to evaluate the overall flavor of RBIDF and SRBIDF samples during different storage time. Fig. 11 showed the radar chart of the ten E-nose sensor response signals of RBIDF and SRBIDF samples. Before adsorption of red date flavoring agent, the response values of ten sensors of RBIDF and SRBIDF samples were low, indicating that the endogenous flavor of RBIDF and SRBIDF was weak and did not have a significant effect on the overall odor profile. After adsorption of red date flavoring agent, the flavor components of RBIDF and SRBIDF samples at different storage time had approximately the same response type to the sensors, indicating similar flavor compositions, but there were differences in the response values corresponding to each sensor, especially on the sensors W1W, W5S, W2W, W1S and W2S, which indicated the differences in the flavor compounds of these samples. It can be seen in Fig. 11 that the response values of W1W, W5S, W2W, W1S, W2S of RBIDF and SRBIDF samples showed gradually decreasing trend with the extension of storage time. However, the decreasing degree of sensor responses of W1W, W5S, W2W, W1S, W2S in SRBIDF samples were lower compared to those in RBIDF samples, this might be due to the enhanced controlled release effect resulted from the steam explosion treatment.

PCA analysis of E-nose data was performed in order to further analyze the flavor difference of RBIDF and SRBIDF samples at different storge time. The two-dimensional and three-dimensional PCA of the E-nose data of RBIDF and SRBIDF samples were presented in Fig. 12. PC1, PC2 and PC3 explained 95.4% of the total variance, which indicated that the extracted principal component factors could reflect the overall characteristics of flavor compounds of the samples. Before flavor adsorption, RBIDF and SRBIDF occupied a relatively independent space in the principal component space and they were separate from the

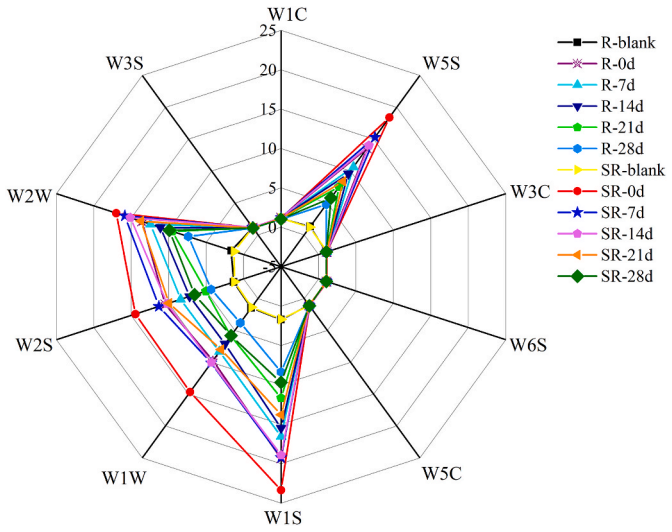

Fig. 11. Radar chart of the e-nose sensor response signals of RBIDF and SRBIDF samples. R-blank and SR-blank represented the RBIDF and SRBIDF samples before flavor adsorption.

samples after flavor adsorption, which indicated the differences in flavor compounds before and after the adsorption of red date flavoring agent. Sample points of SRBIDF at day 0 were located in the positive region of PC1, PC2 and PC3 axes. As storage proceeded, the SRBIDF samples at day 7, day 14, day 21 and day 28 were far away from the sample at day 0. Similar variation was observed in RBIDF samples. In addition, sample points of SRBIDF at day 0, day 7 and day 14 were far away from those of RBIDF samples at day 0, day 7 and day 14 along PC 1 and PC 3 axes, indicating significant differences in the overall flavor characteristics of RBIDF and SRBIDF during 14 days of storage. However, as storage proceeded, sample points of SRBIDF at day 21 and day 28 were closer to those of SRBIDF at day 21 and day 28. These results were consistent with those from cluster analysis of the GC-MS data, further indicating that the differences in flavor release characteristics between RBIDF and SRBIDF samples could be effectively identified by E-nose.

4. Conclusion

The flavor compounds adsorption and controlled release performances of rice bran insoluble dietary fiber modified by steam explosion method were investigated in current study. We found that after steam explosion treatment SRBIDF had a loosened and unfolding inner structure and increased pore structure, and the SSA and PV of SRBIDF increased by 2.96 and 3.28 times respectively compared with those of RBIDF. The pore structure of SRBIDF was mainly slit-like and cylinder pores with porosity mainly in the mesopore range. In addition, result of FTIR spectra showed that the steam explosion treatment caused the exposure of more functional groups of RBIDF, which were beneficial for the flavor-binding ability. The mechanism of adsorption of SRBIDF to flavor compounds was preliminarily explored using adsorption kinetics and isotherms combined with SEM and DSC analysis. The Langmuir isotherm model and pseudo-second-order kinetic model yielded the best fit to the adsorption data, indicating monolayer adsorption of flavor onto SRBIDF, and the adsorption was mainly driven by chemisorption process. SEM and DSC analyses further proved that the flavor compounds were successfully adsorbed and entrapped in the holes and surface of SRBIDF. The adsorption resulted in an improvement of thermal stability and reduction of volatility of flavor compounds, accounting for the ability of SRBIDF to retain the flavor compounds. The flavor release property of RBIDF was investigated by HS-SPME GC/MS and E-nose, and the results showed that the release amount of flavor compounds gradually decreased with the advancement of storage period. After long-time storage, the flavor compounds were retained at a higher concentration in SRBIDF than in RBIDF, indicating enhanced retention and controlled release capacities of SRBIDF for the flavor compounds. The increased porosity and exposure of more binding sites after steam explosion treatment could improve the flavor adsorption ability and flavor retention and sustained release properties from RBIDF. This study provides indications for potential applications of steam explosion-modified RBIDF as a flavor delivery system, which could be added into foods like bakeries, meat or dairy products to enhance their sensory attribute and solve dietary fiber deficiency in human diet. Moreover, it greatly improves the utilization rate of rice bran in functional food.

CRediT authorship contribution statement

Hongcheng Liu: Conceptualization, Validation, Methodology, Formal analysis, Visualization, Investigation, Writing – review & editing, Writing – original draft. **Dilinuer Ainiwan:** Conceptualization, Validation, Methodology, Formal analysis, Visualization, Investigation, Writing – review & editing, Writing – original draft. **Yingxu Liu:** Investigation. **Xiaolan Dong:** Investigation. **Hongxiu Fan:** Investigation. **Tong Sun:** Resources. **Pingyun Huang:** Resources. **Shanshan Zhang:** Writing – review & editing. **Dawei Wang:** Writing – review & editing. **Tingting Liu:** Conceptualization, Supervision, Writing – review & editing, Funding acquisition, Project administration. **Yanrong Zhang:** Writing – review & editing, Supervision.

Declaration of competing interest

The authors declare that they have no personal relationships or known competing financial interests that could have appeared to influence the work reported in this paper.

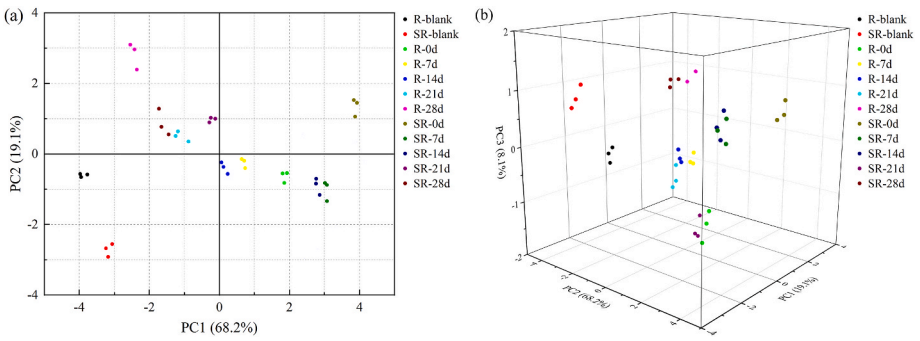

Fig. 12. Two-dimensional (a) and three-dimensional (b) PCA of the E-nose data of RBIDF and SRBIDF samples. R-0d, R-7d, R-14 d, R-21 d, R-28 d represented the RBIDF samples stored for 0, 7, 14, 21, and 28 days, respectively; RS-0d, RS-7d, RS-14 d, RS-21 d, RS-28 d represented the SRBIDF samples stored for 0, 7, 14, 21, and 28 days, respectively. R-blank and SR-blank represented the RBIDF and SRBIDF samples before flavor adsorption.

Data availability

No data was used for the research described in the article.

Acknowledgements

This work was financially supported by the Science and Technology Rearch Project of the Education Department of Jilin Province (Grant No. JJKH20210344KJ), Science and Technology Development Plan project of Jilin Province (Grant Nos. 20210508014RQ, 20200403165SF and 20200502001NC). We would like to thank Editage (www.editage.cn) for English language editing.

References

Ali, N.S., Jabbar, N.M., Alardhi, S.M., Majdi, H.S., Albayati, T.M., 2022. Adsorption of methyl violet dye onto a prepared bio-adsorbent from date seeds: isotherm, kinetics, and thermodynamic studies. Heliyon 8, e10276. https://doi.org/10.1016/j.heliyon.2022.e10276.

Barrett, E., Joyner, L., Halenda, P., 1951. The determination of pore volume and area distributions in porous substances. I. Computations from nitrogen isotherms. J. Am. Chem. Soc. 73, 373–380. https://doi.org/10.1021/ja01145a126.

Bayrac, C., Yilmaz, B., Bayrakci, M., 2022. Adsorption behavior of carboxy- and amine-terminated magnetic beads for patulin: batch experiments in aqueous solution and apple juice. Food Res. Int. 162, 112077 https://doi.org/10.1016/j.foodres.2022.112077.

Brunauer, S., Emmett, P.H., Teller, E., 1938. Adsorption of gases in multimolecular layers. J. Am. Chem. Soc. 60, 309–319. https://doi.org/10.1021/ja01269a023.

Chen, Y.J., Li, J.N., Wang, F.H., Yang, H., Liu, L., 2021. Adsorption of tetracyclines onto polyethylene microplastics: a combined study of experiment and molecular dynamics simulation. Chemosphere 265, 129133. https://doi.org/10.1016/j.chemosphere.2020.129133.

Chen, X.J., Lin, Q.M., Muhammad, R., Zhao, X.R., Li, G.T., 2019. Steam explosion of crop straws improves the characteristics of biochar as a soil amendment. J. Integr. Agric. 18, 1486–1495. http://creativecommons.org/licenses/by-nc-nd/4.0/.

Chu, G., Zhao, J., Huang, Y., Zhou, D.D., Liu, Y., Wu, M., Peng, H., Zhao, Q., Pan, B., Steinberg, C., 2018. Phosphoric acid pretreatment enhances the specific surface areas of biochars by generation of micropores. Environ. Pollut. 240, 1–9. https://doi.org/10.1016/j.envpol.2018.04.003.

Fan, H., Liu, H., Li, W., Su, W., Wang, D., Zhang, S., Liu, T., Zhang, Y., 2023. Effect of Tremella fuciformis polysaccharide on the stalling and flavor of tteok during storage. Food Sci. Hum. Wellness 12, 254–265. https://doi.org/10.1016/j.fshw.2022.07.005.

Han, Z., Cai, M., Cheng, J., Sun, D., 2021. Effects of constant power microwave on the adsorption behaviour of myofibril protein to aldehyde flavour compounds. Food Chem. 336, 127728 https://doi.org/10.1016/j.foodchem.2020.127728.

He, L., Wang, C., Shi, H., Zhou, W., Zhang, Q., Chen, X., 2019. Combination of steam explosion pretreatment and anaerobic alkalization treatment to improve enzymatic hydrolysis of Hippophae rhamnoides. Bioresour. Technol. 289, 121693 https://doi.org/10.1016/j.biortech.2019.121693.

Hu, L., Wu, Y., Li, M., Zhang, X., Xian, X., Mai, Y., Lin, X., 2022. Highly selective adsorption of 5-hydroxymethylfurfural from multicomponent mixture by simple pH controlled in batch and fixed-bed column studies: competitive isotherms, kinetic and breakthrough curves simulation. Sep. Purif. Technol. 299, 121756 https://doi.org/10.1016/j.seppur.2022.121756.

Ishii, R., Imai, Y., Wada, M., Ebina, T., Hanaoka, T., Mizukami, F., 2006. Adsorption and desorption behaviors of flavor molecules into a microporous pillared clay mineral and the application to flavor capsule composites. Appl. Clay Sci. 33, 99–108. https://doi.org/10.1016/j.clay.2006.04.009.

Khamwichit, A., Dechapanya, W., Dechapanya, W., 2022. Adsorption kinetics and isotherms of binary metal ion aqueous solution using untreated venus shell. Heliyon 8, e09610. https://doi.org/10.1016/j.heliyon.2022.e09610.

Li, Q., Liu, R., Wu, T., Zhang, M., 2017. Interactions between soluble dietary fibers and wheat gluten in dough studied by confocal laser scanning microscopy. Food Res. Int. 9, 19–27. https://doi.org/10.1016/j.foodres.2017.02.021.

Li, T., Wang, L., Chen, Z., Li, C., Li, X., Sun, D., 2020. Structural changes and enzymatic hydrolysis yield of rice bran fiber under electron beam irradiation. Food Bioprod. Process. 122, 62–71. https://doi.org/10.1016/j.lwt.2021.111172.

Li, Z., Liu, D., Cai, Y., Wang, Y., Teng, J., 2019. Adsorption pore structure and its fractal characteristics of coals by N_2 adsorption/desorption and FESEM image analyses. Fuel 257, 116031. https://doi.org/10.1016/j.fuel.2019.116031.

Liu, S., Li, S., Ho, C., 2022. Dietary bioactives and essential oils of lemon and lime fruits. Food Sci. Hum. Wellness 11, 753–764. https://doi.org/10.1016/j.fshw.2022.03.001.

Liu, X., Suo, K., Wang, P., Li, X., Hao, L., Zhu, J., Yi, J., Kang, Q., Huang, J., Lu, J., 2021. Modification of wheat bran insoluble and soluble dietary fibers with snail enzyme. Food Sci. Hum. Wellness 10, 356–361. https://doi.org/10.1016/j.fshw.2021.02.027.

Lv, Y., Zhang, L., Li, M., He, X., Hao, L., Dai, Y., 2019. Physicochemical properties and digestibility of potato starch treated by ball milling with tea polyphenols. Int. J. Biol. Macromol. 129, 207–213. https://doi.org/10.1016/j.igbiomac.2019.02.028.

Moreira, B.P., Draszewski, C.P., Rosa, N.C., Tres, M.V., Zabot, G.L., Pereira, F.C., Abaide, E.R., Castilhos, F., 2023. Integrated rice bran processing by supercritical CO_2 extraction and subcritical water hydrolysis to obtain oil, fermentable sugars, and platform chemicals. J. Supercrit. Fluids 192, 105786. https://doi.org/10.1016/j.supflu.2022.105786.

Niu, L., Guo, Q., Xiao, J., Li, Y., Deng, X., Sun, T., Liu, X., Xiao, C., 2023. The effect of ball milling on the structure, physicochemical and functional properties of insoluble dietary fiber from three grain bran. Food Res. Int. 163, 11226 https://doi.org/10.1016/j.foodres.2022.112263.

Niu, Y., Zhu, Q., Xiao, Z., 2021. The aroma composition and synergistic effect among key aroma compounds in Moutai Baijiu. J. Chin. Inst. Food Sci. Technol. 21, 215–226. https://doi.org/10.16429/j.1009-7848.2021.10.024 (in Chinese).

Ouyang, H., Wu, L., Hu, Y., Li, L., Li, Z., He, H., Jiang, Z., Li, Q., Ni, H., Zheng, M., 2023a. Effect of steam explosion treatment on physicochemical, functional and structural properties of pomelo fruitlets. LWT 184, 114963. https://doi.org/10.1016/j.lwt.2023.114963.

Ouyang, H., Guo, B., Hu, Y., Li, L., Jiang, Z., Li, Q., Ni, H., Li, Z., Zheng, M., 2023b. Effect of ultra-high pressure treatment on structural and functional properties of dietary fiber from pomelo fruitlets. Food Biosci. 52, 102436 https://doi.org/10.1016/j.fbio.2023.102436.

Pino, J.A., Mesa, J., 2006. Contribution of volatile compounds to mango (*Mangifera indica* L.) aroma. Flavour Fragrance J. 21, 207–213. https://doi.org/10.1002/ffj.1703.

Premjit, Y., Pandhi, S., Kumar, A., Rai, D.C., Duary, R.K., Mahato, D.K., 2022. Current trends in flavor encapsulation: a comprehensive review of emerging encapsulation techniques, flavour release, and mathematical modelling. Food Res. Int. 151, 110897 https://doi.org/10.1016/j.foodres.2021.110879.

Rezaeinia, H., Emadzadeh, B., Ghorani, B., 2020. Electrospun balangu (Lallemantia royleana) hydrocolloid nanofiber mat as a fast-dissolving carrier for bergamot essential oil. Food Hydrocolloids 100, 105312. https://doi.org/10.1016/j.foodhyd.2019.105312.

Song, J., Wang, L., Zhao, H., Wang, H., Zhang, N., Wang, W., Shen, X., Wu, Y., 2020. Analysis of volatile components in distilled spirits with grape skin residue of different varieties. China Brew. 39, 124–132. https://doi.org/10.11882/j.issn.0254-5071.2020.06.025 (in Chinese).

Sun, B., Chen, H., 2017. The Technology of Food Flavering, third ed. Chemical Industry Press, Beijing, pp. 113–145 (in Chinese).

Sun, B., Zheng, F., Liu, Y., 2000. Perfumes and Essences. China Petrochemical Press, Beijing, pp. 42–78 (in Chinese).

Tong, Z., Zhang, J., Li, Z., Wu, Y., Wang, D., Gong, D., 2022. Investigation of organic-shale nanopores in the Lower Cambrian Niutitang Formation using low temperature N_2 and CO_2 adsorption: multifractality and classification. Microporous Mesoporous Mater. 337, 111935 https://doi.org/10.1016/j.micromeso.2022.111935.

Ullah, I., Khoder, R.M., Yin, T., You, J., Huang, Q.L., Liu, R., Xiong, S., 2023. Gelation properties of tofu induced by different coagulants: effects of molecular interactions between nano-sized okara dietary fiber and soybean proteins. Food Chem. 403, 134056 https://doi.org/10.1016/j.foodchem.2022.134056.

Van Gemert, L.J., 2011. Flavour Thresholds: Compilations of Flavour Threshold Values in Water and Other Media, second ed. Oliemans, Punter&Partners, Zeist, Netherlands.

Vitrone, F., Ramos, D., Vitagliano, V., Ferrando, F., Salvado, J., 2022. All-lignocellulosic fiberboards from giant reed (*Arundo donax* L.): effect of steam explosion pre-treatment on physical and mechanical properties. Construct. Build. Mater. 319, 126064 https://doi.org/10.1016/j.conbuildmat.2021.126064.

Wang, H., Qiu, C., Song, Y., Bian, S., Wang, Q., Chen, Y., Fang, C., 2022. Adsorption of tetracycline and Cd(II) on polystyrene and polyethylene terephthalate microplastics with ultraviolet and hydrogen peroxide aging treatment. Sci. Total Environ. 845, 157109 https://doi.org/10.1016/j.scitotenv.2022.157109.

Wang, W., Yang, B., Li, W., Zhou, Q., Liu, C., Zheng, C., 2021. Effects of steam explosion pretreatment on the bioactive components and characteristics of rapeseed and rapeseed products. LWT 143, 111172. https://doi.org/10.1016/j.lwt.2021.111172.

Wu, Q., Ren, M., Zhang, X., Li, C., Li, T., Yang, Z., Chen, Z., Wang, L., 2021a. Comparison of Cd(II) adsorption properties onto cellulose, hemicellulose and lignin extracted from rice bran. LWT 144, 111230. https://doi.org/10.1016/j.lwt.2021.111230.

Wu, Q., Wu, J., Ren, M., Zhang, X., Wang, L., 2021b. Modification of insoluble dietary fiber from rice bran with dynamic high pressure microfluidization: Cd(II) adsorption capacity and behavior. Innov. Food Sci. Emerg. 73, 102765 https://doi.org/10.1016/j.ifset.2021.102765.

Xia, Q., Mei, J., Yu, W., Li, Y., 2017. High hydrostatic pressure treatments enhance volatile components of pre-germinated brown rice revealed by aromatic fingerprinting based on HS-SPME/GC-MS and chemometric methods. Food Res. Int. 91, 103–114. https://doi.org/10.1016/j.foodres.2016. 12.001.

Xiao, Y., Huang, Y., Chen, Y., Xiao, L., Zhang, X., Yang, C., Li, Z., Zhu, M., Liu, Z., Wang, Y., 2022. Discrimination and characterization of the volatile profiles of five Fu brick teas from different manufacturing regions by using HS–SPME/GC–MS and HS–GC–IMS. Curr. Res. Food Sci. 5, 1788–1807. https://doi.org/10.1016/j.crfs.2022.09.024.

Xu, Y., Lv, Y., Yin, Y., Zhao, H., Li, X., Yi, S., Li, J., 2022. Improvement of the gel properties and flavor adsorption capacity of fish myosin upon yeast β-glucan incorporation. Food Chem. 397, 133766 https://doi.org/10.1016/j.foodchem.2022.133766.

Xu, Y., Li, T., Li, L., Chen, Y., Hu, Y., Jiang, Z., Yang, Y., Ni, H., Huang, G.L., 2019. Ananlysis of volatile components in the instant Dianhong tea by SDE-GC-MS and GC-O. Modern Food Science and Technology 35, 277–284+276. https://doi.org/10.13982/j.mfst.1673-9078.2019.11.038 (in Chinese).

Yadav, B.S., Dasgupta, S., 2022. Effect of time, pH, and temperature on kinetics for adsorption of methyl orange dye into the modified nitrate intercalated MgAl LDH adsorbent. Inorg. Chem. Commun. 137, 109203 https://doi.org/10.1016/j.inoche.2022.109203.

Yi, M., Cheng, Y., Wang, Z., Wang, C., Hu, B., He, X., 2020. Effect of particle size and adsorption equilibrium time on pore structure characterization in low pressure N_2 adsorption of coal: an experimental study. Adv. Powder Technol. 31, 4275–4281. https://doi.org/10.1016/j.apt.2020.09.004.

Zhang, Z., Chen, Z., Zhang, C., Kang, W., 2023. Physicochemical properties and biological activities of Tremella hydrocolloids. Food Chem. 407, 135164 https://doi.org/10.1016/j.foodchem.2022.135164.

Zhao, G., Zhang, R., Dong, L., Huang, F., Tang, X., Wei, Z., Zhang, M., 2018. Particle size of insoluble dietary fiber from rice bran affects its phenolic profile, bioaccessibility and functional properties. LWT 87, 450–456. https://doi.org/10.1016/j.lwt.2017.09.016.

Zhao, Y., Wei, W., Tang, L., Wang, D., Wang, Y., Wu, Z., Zhang, W., 2021. Characterization of aroma and bacteria profiles of Sichuan industrial paocai by HS-SPME-GC-O-MS and 16S rRNA amplicon sequencing. Food Res. Int. 149, 110667 https://doi.org/10.1016/j.foodres.2021.110667.

Zheng, A.R., Wei, C.K., Liu, D.H., Thakur, K., Zhang, J.G., Wei, Z.J., 2023. GC-MS and GC×GC-TOF-MS analysis of roasted/broth flavors produced by Maillard reaction system of cysteine-xylose-glutamate. Curr. Res. Food Sci. 6, 100445 https://doi.org/10.1016/j.crfs.2023.100445.

Zhou, B., Yang, S., Jiang, X., Song, W., 2023. Experimental study on oxygen adsorption capacity and oxidation characteristics of coal samples with different particle sizes. Fuel 331, 125954. https://doi.org/10.1016/j.fuel.2022.125954.